Research Article

The Role of CH$_4$ in Plasma-Assisted CO$_2$ and CH$_4$ Conversion in a Rotating Gliding Arc Plasma: Insights Revealed by Experiments and Modeling

Senne Van Alphen,*,§ Bart Wanten,§ Fanny Girard-Sahun,§ Joachim Slaets,§ James Creel, Maryam Aghaei, and Annemie Bogaerts*

Cite This: *ACS Sustainable Chem. Eng.* 2024, 12, 15715−15728

Read Online

ACCESS | Metrics & More | Article Recommendations | SI Supporting Information

ABSTRACT: We investigated the combined conversion of CO$_2$ and CH$_4$, so-called dry reforming of methane (DRM), in a rotating gliding arc (RGA) reactor by experiments and modeling for different CO$_2$/CH$_4$ mixing ratios. We obtained the best results at the lowest flow rate (4 L/min) and the lowest amount of CH$_4$ in the feed gas mixture (25%), reaching a conversion of 22% and 39% for CO$_2$ and CH$_4$, respectively, an energy efficiency of 62% and energy cost of 3.25 eV/molecule. A lower energy cost of 2.65 eV/molecule was obtained at 8 L/min. By means of a 3D computational fluid dynamics model, we show that the addition of CH$_4$ reduces the gas temperature inside the plasma, resulting in slower chemical kinetics, explaining why the least amount of CH$_4$ (i.e., 25/75 CH$_4$/CO$_2$) yields the highest CO$_2$ and CH$_4$ conversion. Additionally, the 25/75 CH$_4$/CO$_2$ mixture also displays the highest energy efficiency, due to the high conversion, as well as due the high CO concentration produced in this gas mixture, which is the most beneficial product in terms of energy efficiency. Finally, by means of a quasi-1D chemical kinetics model, we demonstrate that the addition of CH$_4$ suppresses the CO recombination reactions back into CO$_2$, after the plasma, as H-based radicals from CH$_4$ quickly react with O radicals that would otherwise recombine with CO.

KEYWORDS: Plasmatechnology, dry reforming of methane, sustainable CO$_2$ conversion, CCU, Computational fluid dynamics, plasmamodeling
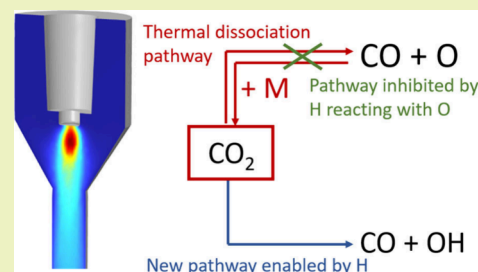
1. INTRODUCTION

The increasing emission of greenhouse gases such as CO$_2$ due to oil combustion, deforestation and fossil fuel consumption is known to play a major role in the actual global warming.[1] As the demand for energy is growing worldwide, we need to invest more in renewable energy sources, while reducing greenhouse gas concentrations in the earth atmosphere. The conversion of CO$_2$ together with CH$_4$ (e.g., from biogas) into value-added chemicals can contribute to meet these needs. This could be achieved by the dry reforming of methane (DRM) reaction:[2]

$$CO_{2(g)} + CH_{4(g)} \rightarrow 2CO_{(g)} + 2H_{2(g)}$$
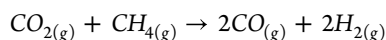
with $\Delta H° = +247 \; kJ.\,mol^{-1}$

This chemical reaction is highly endothermic, so elevated temperatures are required (≈ 1000 K)[3] for a good efficiency. DRM is usually performed by catalytic processes,[4] but major issues of coke deposition and catalyst deactivation make this approach not yet suitable for commercial application.[3]

An alternative technology is based on gas discharge plasma,[3] a partially ionized gas, usually generated by applying a sufficient electric field in a working gas flowing between two electrodes. The naturally present light electrons are easily accelerated by the electric field, they collide with the gas molecules, giving rise to ionization, excitation and dissociation, producing, in the end, a rich mixture of electrons (with higher temperature than the other species), various ions, radicals, atoms and molecules, both in the ground state and excited levels, including electronically, vibrationally and rotationally excited.[5] Vibrationally excited molecules can play an important role in plasma chemical kinetics, depending on the type of plasma, because in theory they can give rise to the most efficient conversion by vibrationally excited dissociation (so-called ladder climbing).[3,5] Moreover, plasmas are typically generated at atmospheric pressure and the gas enters at room temperature (although it can be efficiently heated to several 1000 K inside the plasma reactor, resulting in mainly thermal chemistry). Finally, this process can be easily turned ON/OFF, making it very suitable to be combined with fluctuating renewable electricity.[3]
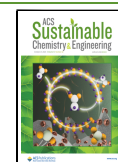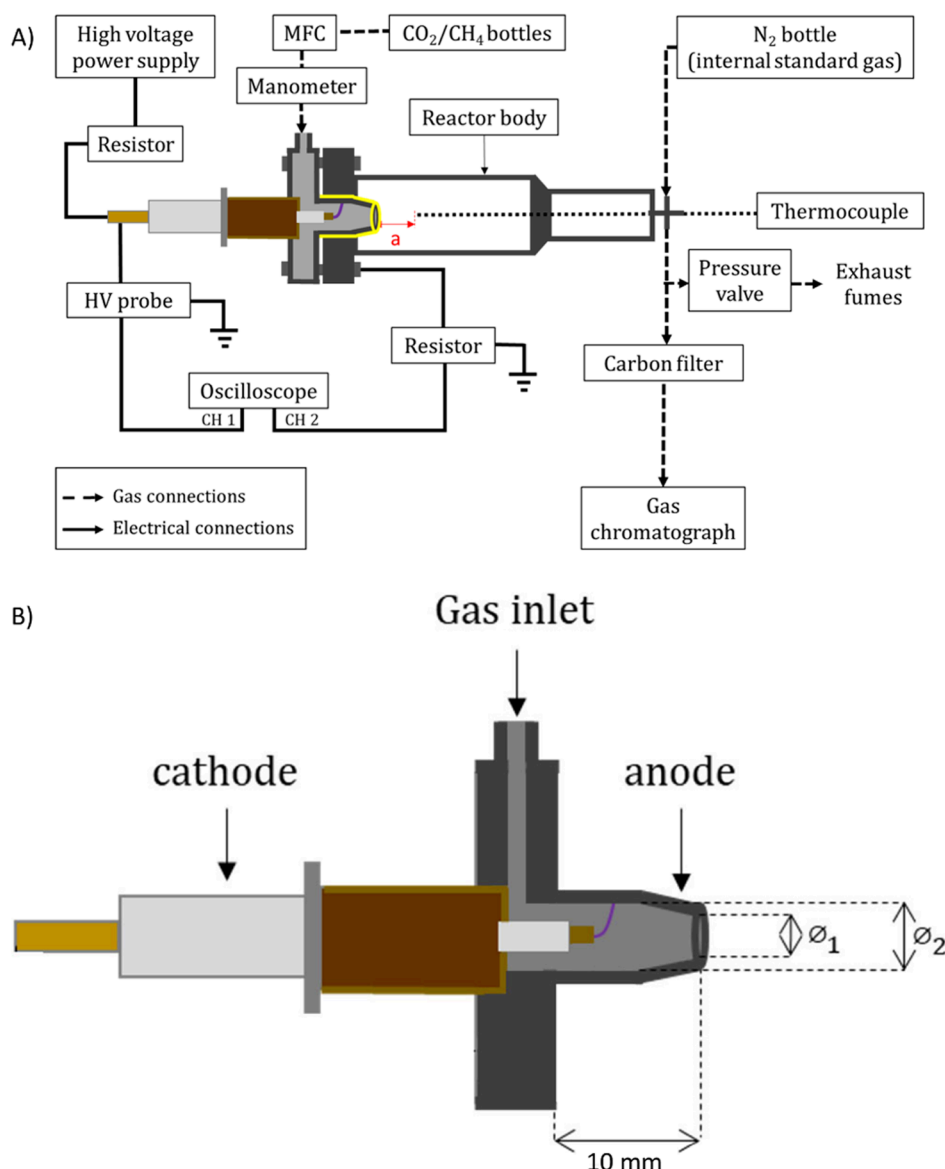
Figure 1. A) Scheme of the experimental setup, including the RGA reactor and a gas chromatograph (GC) for analyzing the gas composition after passing through the reactor. The power supply delivers a DC current, preset at 100 mA. The flow rate was varied (4−6−8 L/min) for various gas mixtures (CH_4/CO_2 with either 25−33−40% CH_4). A thermocouple was inserted in the reactor body, at a characteristic distance a = ± 3 cm. B) Detailed scheme of the electrodes. The cathode is inserted into the anode, which has a conical outlet (inner diameter $\varnothing_1$ = 2 mm and outer diameter $\varnothing_2$ = 6.5 mm). The gas is introduced tangentially through the anode, ensuring a vortex flow around the conical part, to pull the rotating arc toward the outlet.

Various plasma types have been studied for DRM over the last decades, such as dielectric barrier discharges (DBDs),[6,7] atmospheric pressure glow discharges (APGDs),[8,9] microwave (MW)[10−12] or gliding arc (GA) discharges.[13−18] The latter are of great interest because: (1) the electron temperature is around 1 eV, necessary for efficient excitation of CO_2 vibrational levels, and (2) the electron density is usually higher than in some other plasma types mentioned above ($10^{23}−10^{24}$ m^{-3}).[19] GA reactors were originally made of two diverging blade electrodes[3,19,20] (2D geometry), where the arc is first formed at the narrowest gap between the two electrodes in a quasi-equilibrium state, and then dragged between both electrodes toward the upper part due to the gas flow. This transition is fast and followed by an evolution in a nonequilibrium regime, with a high electron temperature (T_e = 1 eV). When the nonequilibrium discharge cannot be sustained anymore (because the distance between both diverging electrodes becomes too large), a new breakdown can occur and the phenomenon is repeated.[21] Therefore, GA discharges take advantage of both thermal and nonthermal plasmas (high nonequilibrium level) and provide high temperature as well as high electron density at atmospheric pressure.[20]

In recent years, classical GA reactors have been improved into a 3D geometry, to overcome some drawbacks.[22] Indeed, the gas fraction passing through the arc is limited due to the 2D geometry and the flow rates needed to sustain the arc gliding mechanism are usually quite high (10−20 L/min), leading to a short gas residence time and thus, low conversion and energy efficiency.[21] In contrast, a 3D configuration is

expected to increase the gas fraction passing through the plasma region by a tangential gas inlet, as well as a longer residence time[3,23] required to enhance the chemical reactions of interest, based on plasma imaging experiments[24] and 3D fluid dynamics simulations of the arc dynamics.[25]

Recently, a novel type of 3D gliding arc geometry, i.e. the rotating gliding arc (RGA), was developed and used for CO_2 and/or CH_4 conversion.[13,26−28] Kuznetsova et al. showed that it was possible to stabilize the arc in its nonequilibrium stage before extinction,[29] which would ensure a longer time for a high reaction rate. In addition, a transverse gas flow and/or the use of a magnetic field have been proposed to elongate and stabilize the arc.[21,26,30,31] While developed for CO_2 and/or CH_4 conversion, this type of RGA has also achieved promising results for plasma-based nitrogen fixation.[32−34] In these studies, an RGA reactor was used for converting N_2 and O_2 into NO_x, serving as a precursor for sustainable fertilizer production, achieving very high NO_x concentrations up to 5.5% with an energy consumption of 2.5 MJ/mol.[34] The performance of the RGA reactor was even further increased when the reactor was equipped with an effusion nozzle for postplasma gas quenching, yielding NO_x concentrations up to 5.9%, at an energy cost down to 2.1 MJ/mol.[33]

In the present work, we studied the performances of an RGA reactor fed with a tangential gas flow, for DRM. We varied the gas flow rate and the CO_2/CH_4 ratio, in order to identify the best combination leading to the highest conversion, energy efficiency and product selectivity, in particular for syngas (CO, H_2) and C_2H_x compounds. In addition, we developed both a 3D computational fluid dynamics (CFD) model and a quasi-1D chemical kinetics model to reveal the underlying physical and chemical mechanisms inside the reactor and explain the observed experimental trends.

2. EXPERIMENTAL SETUP

2.1. Plasma Setup and Electrical Diagnostics. A global schematic of the RGA setup is presented in Figure 1 A. The cathode, made of stainless steel (100 mm in length, 3 mm in radius) is inserted inside the grounded hollow electrode (anode) and supplied by a high voltage current-controlled power supply (TOPOWER). A more detailed scheme of the electrode configuration is shown in Figure 1 B. In order to limit and stabilize the current, a resistor 25 kΩ was connected to the power supply. The operating current was preset at 100 mA. In addition, a ceramic cap (yellow in Figure 1 A) is placed over the anode to provide electrical insulation between the anode and the reactor body.

We analyzed the electrical signals from the discharge by means of an oscilloscope (Tektronix) equipped with a specific high voltage probe for measuring the voltage, while the current was measured from the anode through a resistor (25 Ω) and calculated by means of Ohm's law. The voltage probe was clamped around the cathode and connected to Channel 1 of the oscilloscope, while Channel 2 was connected to the outer part of the anode (see Figure 1 A). Thereafter, the power was calculated based on the voltage and current values recorded by the oscilloscope.

The working gas is injected through a tangential inlet in the anode in order to provide a vortex flow into its conical part. We tested various CH_4/CO_2 gas mixtures. The mixing ratio was adjusted by mass flow controllers (Bronkorst), with various CH_4 amounts of 25%, 33% and 40%. The flow rate was also varied (4−6−8 L/min) and checked before entering the anode with a manometer.

2.2. Gas Chromatography Measurements. In order to analyze the chemical composition of the gas after passing through the RGA reactor, we placed a gas chromatograph (Thermo Scientific trace 1310 GC) after the exhaust of the reactor, equipped with a thermal conductivity detector (TCD). We placed a carbon filter before the GC entrance to avoid any carbon contamination (Figure 1 A). As the GC works at atmospheric pressure, a pressure valve was needed to adjust the pressure of the gas before entering the GC. The extra gas was directed to the fume-hood into which the reactor is installed. After plasma was turned ON, the GC was filled with gas, and we waited 10 min to get a stabilized plasma. Each condition was performed in triplicate, each consisting of a set of four GC measurements. For every condition, we measured the most important products, i.e., CO, H_2, and C_2H_x. The absolute conversion (X_{abs}) was calculated as

$$X_{abs_{CO_2}}(\%) = \left(1 - \frac{\alpha \cdot c_{CO_2}^{out}}{c_{CO_2}^{in}}\right) \cdot 100 \tag{1}$$

$$X_{abs_{CH_4}}(\%) = \left(1 - \frac{\alpha \cdot c_{CH_4}^{out}}{c_{CH_4}^{in}}\right) \cdot 100 \tag{2}$$

In which c^{in} is the concentration of the species at the inlet and c^{out} the concentration of the species at the outlet, determined by the average of the peak areas from the four sample loops that were analyzed by the GC, and α is a correction factor for gas expansion.[16,35] This factor is required as the DRM reaction leads to an increasing number of molecules, and thus expansion of the gas and an increase in the volumetric flow rate.

The expansion factor can be determined by adding an internal standard, here N_2 (purity 99.9%), to the outflow gas stream after the gas has passed through the reactor (i.e., 10% of the outlet flow rate, or $\beta = 0.1$). The factor α is defined as the ratio of the peak area of this internal standard from the blank to the plasma measurement, and depends on the factor β, which accounts for the increased gas flow rate because of the internal standard:[16,35]

$$\alpha = \frac{A_{blanc}}{A_{plasma}}(1 + \beta) - \beta \tag{3}$$

$$\beta = \frac{Q_{N_2}(L\ min^{-1})}{Q_{plasma}(L\ min^{-1})} \tag{4}$$

This gas expansion is inherent to DRM, where potentially the number of moles increases by a factor 2 (as shown in the Introduction). This value depends on the reaction stoichiometry at a specific condition, as well as the conversion of the reactants. Generally, the value for the factor α is in the range between 1 and 2.[9,12,17,36] This factor is also taken into account when measuring concentrations, both during the blank measurements, as well as the plasma experiments:

$$c^{blanc} = c_m^{blanc}(1 + \beta) \tag{4a}$$

$$c^{plasma} = c_m^{plasma}\left(1 + \frac{\beta}{\alpha}\right) \tag{5}$$

The specific energy input (SEI) is calculated through:

$$SEI\ (kJ\ L^{-1}) = \frac{P_{plasma}\ (kW) \cdot 60\ (s\ min^{-1})}{\Phi_{flow}\ (L\ min^{-1})} \tag{6}$$

$$SEI\ (eV\ molecule^{-1})$$
$$= SEI\ (kJ\ L^{-1}) \cdot \frac{6.24 \times 10^{21}\ (eV\ kJ^{-1}) \cdot V_{mol}(L\ mol^{-1})}{6.022 \times 10^{23}\ (molecule\ mol^{-1})} \tag{7}$$

In which P_{plasma} is the plasma power calculated from the oscilloscope, connected to the high-voltage (HV) probe in Figure 1A, V_{mol} is the molar volume (24.5 L mol^{-1} at 293 K) and Φ_{flow} is the total gas flow. The energy cost of the conversion (EC), both in kJ/L and eV/molecule, is calculated from the total conversion as

$$EC \ (kJ/L) = \frac{SEI \ (kJ/L)}{X_{total}} \tag{8}$$

$$EC \ (eV/molecule) = EC \ (kJ/L) \cdot$$
$$\frac{6.24 \times 10^{21} \ (eV \ kJ^{-1}) \cdot V_{mol} \ (L/mol)}{6.022 \times 10^{23} \ (molecule/mol)} \tag{9}$$

The energy efficiency (EE) of the conversion process is then calculated using the formula proposed by Van Wanten et al.,[35] describing the fraction of the applied energy that is actually used in the plasma process to break and form chemical bonds rather than being wasted e.g. as heat:

$$EE = \frac{\alpha \cdot (c_{CO}^{out} \cdot LHV_{CO} + c_{H_2}^{out} \cdot LHV_{H_2} + c_{H_2O}^{out} \cdot LHV_{H_2O})}{SEI \ (kJ \ L^{-1}) + (c_{CO_2}^{in} \cdot LHV_{CO_2} + c_{CH_4}^{in} \cdot LHV_{CH_4})} \tag{10}$$

Here the energy that is intrinsically present in the reactants and product molecules is expressed by a lower heating value (LHV), which is a measure for the energy that is released upon full oxidation of the specified species, the so-called "fuel energy efficiency". For this calculation, the LHV of the reactants and the most important reaction products are accounted for: $LHV_{CO} = 283$ kJ/mol; $LHV_{H_2} = 242$ kJ/mol; $LHV_{H_2O} = 0$ kJ/mol; $LHV_{CO_2} = 0$ kJ/mol; $LHV_{CH_4} = 802$ kJ/mol.[35] Note that the LHV of CO_2 and H_2O equals 0 kJ/mol as these molecules are already in their thermodynamically most stable oxidation product, which is why these terms can be omitted from the equation and the energy efficiency can be calculated without measuring the H_2O concentration in the setup.

3. COMPUTATIONAL DETAILS

3.1. Describing the Gas Flow. To calculate the gas flow behavior and heat transfer within the RGA reactor, we developed a three-dimensional (3D) computational fluid dynamics (CFD) model in COMSOL Multiphysics.[37] The behavior of the gas flowing through the RGA is described using a laminar flow model that solves the following mass continuity and momentum continuity equations for a Newtonian fluid:

$$\rho_g \frac{\partial \vec{u}}{\partial t} + \rho_g (\vec{u} \cdot \nabla)\vec{u} = \nabla \cdot \left[-p\vec{I} + \mu(\nabla\vec{u} + \nabla(\vec{u})^T) \right.$$
$$\left. - \frac{2}{3}\mu(\nabla \cdot \vec{u})\vec{I} \right] + \vec{F} \tag{11}$$

$$\rho_g \frac{\partial \vec{u}}{\partial t} + \nabla \cdot (\rho_g \vec{u}) = 0 \tag{12}$$

Where ρ_g stands for the gas density, $\vec{u}$ is the gas flow velocity vector, superscript T stands for transposition, p is the gas pressure, μ is the dynamic viscosity, $\vec{I}$ the unity tensor and $\vec{F}$ the body force vector (which includes forces like gravity but is considered zero as they are not the driving force of the fluid flow in this model).

3.2. Calculating the Heat Balance. The gas temperature is calculated by solving the heat balance equation, which calculates the transport of heat from the plasma, represented in the equation by a heat source Q_{heat}, through conduction and convection:

$$\rho_g C_p \frac{\partial T_g}{\partial t} + \rho_g C_p \vec{u} \cdot \nabla T_g + \nabla \cdot \vec{q} = Q_{heat} \tag{13}$$

Where ρ_g stands for the gas density, C_p for the isobaric heat capacity, T_g is the gas temperature, $\vec{u}$ the gas velocity, Q_{heat} the

heat source term representing the heating from the plasma, and $\vec{q}$ the conductive heat flux vector, which is calculated by

$$\vec{q} = -k_g \nabla T_g \tag{14}$$

Where k_g is the thermal conductivity of the gas

The reason that we represent the plasma as a general heat source Q_{heat} is to save computation time, and because it can reasonably describe the processes of interest in a quasi-thermal plasma.[16,33,38]

Q_{heat} is calculated using two different parameters, i.e. (i) the amount of power transferred to gas heating (P_{heat}, in W) and (ii) the plasma volume (V_{plasma}, in m^3), such that the ratio of both yields the power density (Q_{heat}, in W/m^3):

$$Q_{heat} = \frac{P_{heat}}{V_{plasma}} \tag{15}$$

P_{heat} represents the gas heating that occurs because of exothermic chemical reactions, including relaxation reactions of excited species. In quasi-thermal plasmas at atmospheric pressure, like our RGA, it is reasonable to assume that all the power absorbed by the electrons that did not go into chemical reactions is nearly fully transferred to gas heating.[5,39,40] This allows the plasma power transferred to heating to be calculated using the experimental plasma power P_{plasma}, which is calculated using the voltage−current characteristics of the plasma setup measured by the oscilloscope (see section 2.1), and the experimental energy efficiency EE, which is calculated from the concentrations of the plasma products at the outlet (see eq 10 in section 2.2):

$$P_{heat} = P_{plasma}(100\% - EE) \tag{16}$$

For V_{plasma}, we assume that the arc has the shape of a cylinder with length of 7.85 mm and diameter of 2 mm. The length is based on the distance between anode and cathode, while the diameter is based on previous simulation work by our group.[32−34] Note that this estimation of the power deposited into gas heating is an approximation, and a fully coupled model description will be better suited to describe the gas heating. The reason for using this implementation is to reduce the computational cost of the model, such that 3D solutions could be feasible.

3.3. Properties of the Gas Mixture. As gas molecules undergo chemical transformations in the plasma, the gas composition, and thus also the physical properties of the gas, change throughout the reactor. These effects are accounted for in our simulations by calculating the influence of the chemistry on thermodynamic and transport properties of the gas that are important to the CFD calculation, i.e. the gas density (ρ_g), the heat capacity (C_p), heat conductivity (k_g) and viscosity (μ). We calculate these properties for the different CO_2/CH_4 mixtures over a wide range of gas temperatures (293−4000 K), using the Gri-mech 3.0 database,[41] assuming thermal equilibrium composition at each temperature. This approach circumvents the need for a 3D simulation including coupled chemistry, but a few important approximations are necessary. The assumed thermal equilibrium at each temperature neglects the kinetic aspect of the DRM chemistry, the diffusive transport and the convective transport in and near the plasma. These phenomena do not only affect the chemical composition, which is not calculated in the 3D model, but also the heat transfer in the plasma and consequently the flow (see eq 13), which is included in the 3D model. Establishing a
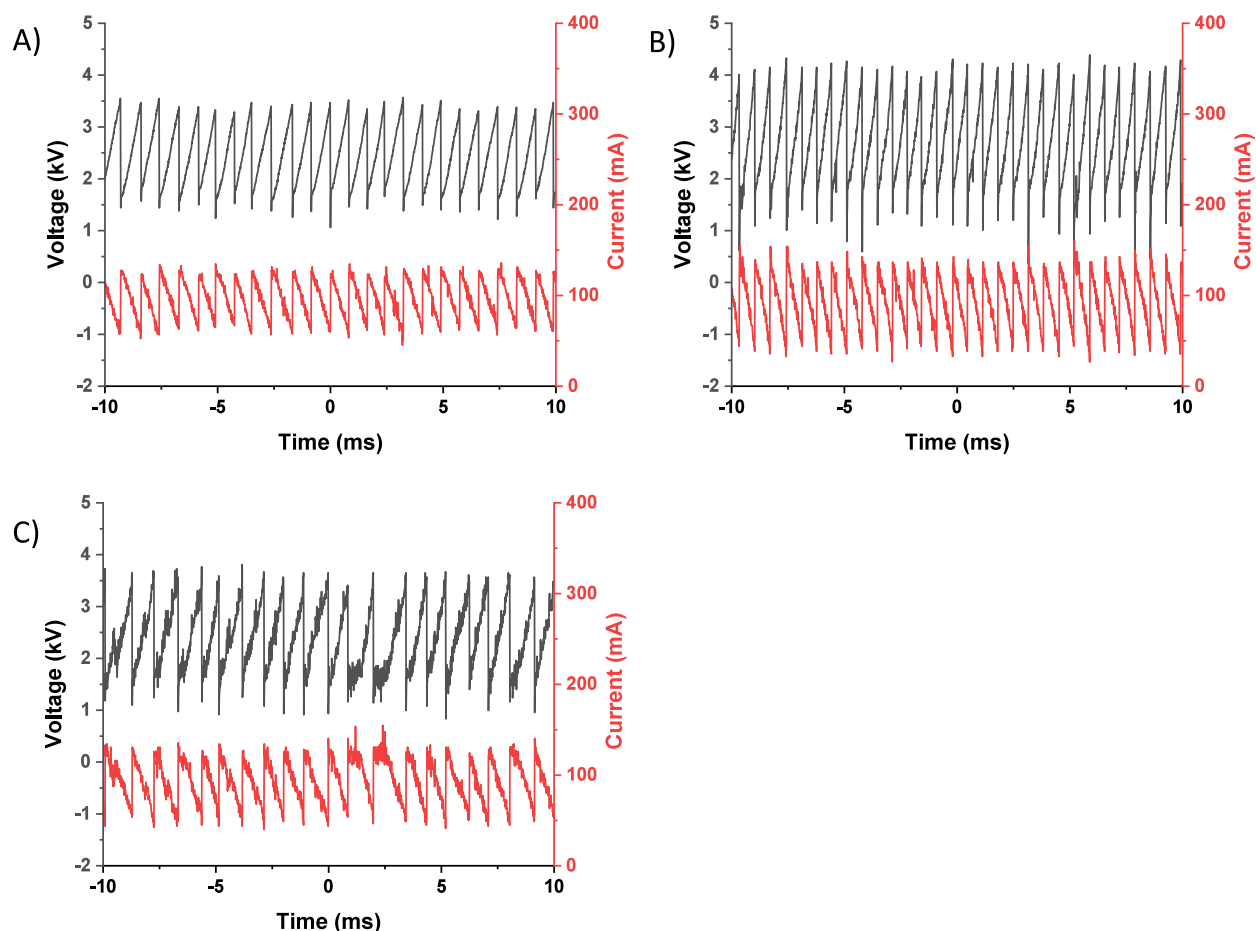
Figure 2. Measured current−voltage waveforms for different CH_4 fractions and different total input flow rates, i.e. (A) 25% CH_4 and 4 L/min, (B) 25% CH_4 and 8 L/min, and (C) 40% CH_4 and 4 L/min.

fully coupled 3D model however lies out of the scope of this research, as it would only benefit when additional experimental data is available to validate the model, such as temperature measurements.

For these look-up tables, C_p is calculated using[42]

$$C_p = \sum_i \omega_i \times \frac{C_{p,i}}{M_i} \tag{17}$$

In which ω_i is the weight fraction of each component i in the mixture at its equilibrium concentration at a given temperature and $C_{p,i}$ is the heat capacity at constant pressure for each of those species.

k_g can be expressed as[42]

$$k_g = 0.5 \left(\sum_i x_i k_i + \frac{1}{\sum_i x_i/k_i} \right) \tag{18}$$

Here, x_i is the molar fraction of species i in the gas mixture and k_i is the thermal conductivity of species i, which is calculated using[42−45]

$$k_i = 2.669 \times 10^{-6} \frac{\sqrt{TM_i \times 10^3}}{\sigma_i^2 \Omega_k} \times \frac{1.15C_{p,i} + 0.88R_g}{M_i} \tag{19}$$

σ_i is the characteristic length of the Lennard-Jones potential of species i, and Ω_k is the dimensionless collision integral given by[42,44,45]

$$\Omega_k = \frac{b_1}{(T^*)^{b_2}} + \frac{b_3}{\exp(b_4 T^*)}$$
$$+ \frac{b_5}{\exp(b_6 T^*)} + \frac{4.998 \cdot 10^{-40} \mu_{D,i}^4}{k_b^2 T^* \sigma_i^6}, \quad T^* = T\frac{\varepsilon_i}{k_b} \tag{20}$$

Here, b_x are empirical constants, $\mu_{D,i}$ is the dipole constant of species i, ε_i is the potential energy minimum value, and k_b is the Boltzmann constant. These values are tabulated data taken from literature.[42]

μ is calculated using[42,46]

$$\mu = \sum_{i=1}^n \frac{\mu_i}{1 + \frac{1}{x_i}\sum_{j=1,j\neq i}^n x_j \phi_{ij}},$$
$$\phi_{ij} = \frac{(1 + (\mu_i/\mu_j)^{0.5}(M_j/M_i)^{0.25})^2}{(4/\sqrt{2})(1 + M_i/M_j)^{0.5}} \tag{21}$$

In this equation, μ_i is the dynamic viscosity of each species i:[42,44,45]

$$\mu_i = 2.669 \times 10^{-6} \frac{\sqrt{TM_i \times 10^3}}{\sigma_i^2 \Omega_D} \tag{22}$$

Here, Ω_D is expressed similar to Ω_k in eq 20, via:[42,44,45]

$$\Omega_D = \frac{b_1}{(T^*)^{b_2}} + \frac{b_3}{\exp(b_4 T^*)} + \frac{b_5}{\exp(b_6 T^*)}$$
$$+ \frac{4.998 \times 10^{-40} \mu_{D,i}^4}{k_b^2 T^* \sigma_i^6}, \qquad T^* = T \frac{k_b}{\varepsilon_i} \tag{23}$$

The gas density of the mixture is calculated using the ideal gas law:[42]

$$\rho_g = \frac{p M_N}{R_g T} \tag{24}$$

This formula uses the pressure, p, the gas constant, R_g, the temperature, T and the mean molar mass of the mixture, M_N.

3.4. Calculating the Underlying Chemistry in a Quasi-1D Chemical Kinetics Model.
To reveal the underlying chemical kinetics in the plasma, we developed a chemical kinetics model that simulates the CO_2/CH_4 chemistry over a one-dimensional straight line in the reactor. While the model calculates the density evolution of the most important plasma species solely as a function of time, like a 0D model, it uses the spatial profile of the calculated gas temperature and gas flow velocity from the above 3D CFD model as input, resulting in a quasi-1D simulation. The evolution of the species densities as a function of time is described by

$$\frac{\partial c_i}{\partial t} = \sum_j a_{ij} r_j \tag{25}$$

in which c_i is the concentration of species i (mol.m^{-3}), and j is the index for the reactions included in the model. The stoichiometric coefficients are denoted as a_{ij}, and are defined as being negative for reactants and positive for products. The reaction rates (r_j, mol/(m^3·s)$^{-1}$) can be described by the mass action law:

$$r_j = k_j^f \prod_i c_i^{-a_{ij}} - k_j^r \prod_i c_i^{a_{ij}} \tag{26}$$

Here, k_j^f and k_j^r represent the forward and reverse rate coefficients, respectively. The rate coefficients of the forward reactions are taken from the Gri-mech 3.0 database,[41] which includes 180 thermal CO_2/CH_4 reactions. The rate coefficients of the reverse reactions are calculated assuming thermodynamic equilibrium:

$$k^r = \frac{k^f}{K_{eq}} \tag{27}$$

In which K_{eq} is the equilibrium constant of the reaction, calculated using thermodynamic constants of the NASA-Glenn database.[47]

The assumption of thermal equilibrium is justified, because in a quasi-thermal plasma operating at atmospheric pressure, the nonequilibrium effects on the heavy particle chemistry are negligible. Indeed, even though species are vibrationally excited upon collision with the electrons in the plasma, the vibrational−translational relaxation collisions occur at such a short time scale at the typical gas temperatures of a quasi-thermal plasma (i.e., around 3000 K), that the chemistry behaves as if in thermal equilibrium.[48]

4. RESULTS AND DISCUSSION

4.1. Electrical Characteristics of the Rotating Arc.
First, it is important to characterize in which mode the RGA is operating. Indeed, previous work showed that an RGA reactor has three distinctive modes, namely the rotating arc mode, the steady arc mode and a transition mode, where in fact the arc alternates between the two aforementioned modes.[32,34] Figure 2 shows the measured current−voltage profiles for (A) 25% CH_4 and 4 L/min, (B) 25% CH_4 and 8 L/min, and (C) 40% CH_4 and 4 L/min. The I−V profiles for the other conditions are added to the SI (section S.1).

The oscillating behavior shown in Figure 2 for both current and voltage indicates that the reactor is operating in the rotating arc mode at the conditions investigated.[32,34] The increase in discharge voltage and decrease in discharge current correspond to the arc elongation, as a consequence of the swirling gas flow. The sudden jumps are indicative of the reignition at the shortest interelectrode distance.

When comparing Figure 2 A and B, we can observe that the frequency of the waveform has clearly increased when applying a higher input flow rate. Indeed, the swirling flow has an even stronger effect on the arc at higher flow rate, and as a result, the arc rotates and extinguishes/reignites much more frequently. Additionally, the higher flow rate increases the length of the arc,[14] which could explain the slightly higher "amplitude" of the peaks in the waveform. Figure 2 A and C show the current−voltage profiles at the same total input flow rate, but a different CH_4 fraction. On first sight, the waveform seems to be less "smooth" in Figure 2 C. We believe this is caused by larger changes in resistivity of the gas mixture at higher CH_4 fractions. For example, soot formation is the most significant at higher CH_4 fractions, which influences the conductivity of the mixture.[9] This is also supported by the fact that a lower overall resistivity is obtained at higher CH_4 fractions, observed in terms of the somewhat lower plasma power at this condition (i.e., 208.2 ± 0.6 W vs 226 ± 1 W at 25% CH_4).

4.2. Surprising Influence of the CO_2/CH_4 Ratio on the CO_2 and CH_4 Conversion.
Figure 3 A and B show the experimental absolute CO_2 and CH_4 conversion, respectively, for three different CO_2/CH_4 mixtures at three different gas flow rates. The highest CO_2 and CH_4 conversions are achieved for a 75/25 CO_2/CH_4 mixture at a flow rate of 4 L/min, yielding a CO_2 conversion of 22.1% and a CH_4 conversion of 38.6%. Note that no experimental results are presented for the 60/40 CO_2/CH_4 ratio at 8 L/min, due to instabilities of the plasma at this particular condition. Also note that the CH_4 conversion is systematically higher than the CO_2 conversion, which is in agreement with literature for the combined CO_2 and CH_4 conversion.[3,49] This is attributed to the double C=O bond of CO_2 requiring more energy to break compared to the single C−H bonds of CH_4.[3] Table 1 compares these results with recent DRM performance metrics of different types of plasmas reported in literature. Although exact comparison is not really possible, because of the somewhat different CH_4/CO_2 mixing ratios, this table shows that our values are competitive with other reactors, outmatching the gliding arc plasmatron (GAP) by Cleiren et al.[17] and the RGA reactor by Martin-del-Campo et al.[14] in terms of conversion, albeit operating at a somewhat higher energy cost than Cleiren et al.,[17] but clearly lower than Marin-del-Campo et al.[14] Also the "rotating gliding arc discharge" (RGAD) reactor of Lu et al.[13]
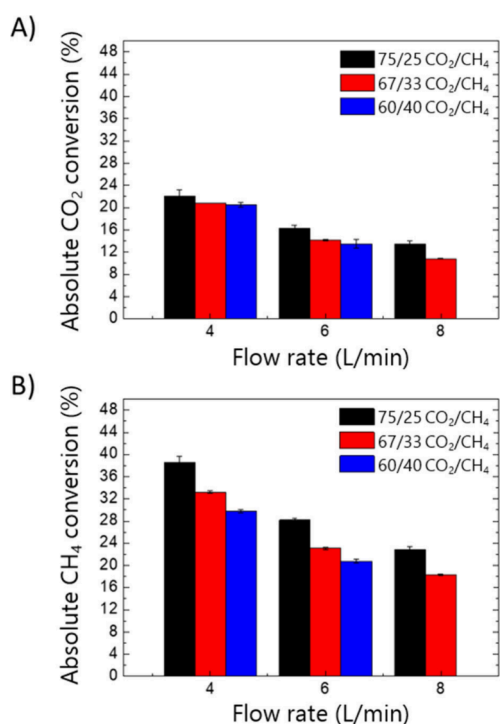
Figure 3. Measured CO_2 (A) and CH_4 (B) conversion for different CO_2/CH_4 mixtures with 25%, 33% and 40% CH_4, at gas flow rates of 4,6 and 8 L/min.

thereby aiming to maximize the amount of gas that is treated by the plasma. Finally, as a reference, the table also shows the performance of three non-GA plasma reactors, i.e. a MW reactor, an APGD reactor and a DBD reactor, which are representative performances for the three reactor types. Similar to a GA plasma, dissociation in both a MW and APGD plasma occurs mainly through efficient thermal reactions, which explains the high conversion achieved in the MW reactor by Kelly et al.[11] and in the APGD reactor by Wanten et al.[9] at a relative low energy cost. Dissociation in a DBD reactor, however, occurs through direct electron impact dissociation, which is less energy efficient. The DBD reactor of Wang et al.[50] achieved a high CO_2 and CH_4 conversion of 44 and 73%, respectively, albeit at a high energy cost of 140 eV/molecule, due to the inefficient dissociation mechanisms of a DBD plasma.

Figure 3 illustrates that both the CO_2 and CH_4 conversions decrease upon rising flow rate, a trend that is expected in plasma reactors. Indeed, higher flow rates result in a shorter residence time inside the chemically active plasma zone and thus less overall conversion by the plasma. A trend that is unexpected, however, is the evolution of the CO_2 and CH_4 conversion as a function of gas composition: Figure 3 indicates that the highest conversions are found at the highest CO_2/CH_4 ratios. One would expect the highest conversions are found at a CO_2/CH_4 ratio close to one, as this is the ideal chemical stoichiometric ratio of CO_2 and CH_4 for the DRM reaction, and the CH_x radicals created by CH_4 dissociation typically contribute to CO_2 splitting.[3,16,17] However, while a CO_2/CH_4 ratio close to one is the most ideal from a chemical point of view, our computational models show that from a physical point of view, a 75/25 CO_2/CH_4 mixture displays far superior conditions for achieving a high CO_2 and CH_4 conversion.

This is illustrated in Figure 4 A−C, where the gas temperature distribution inside the RGA reactor, as calculated by our 3D CFD model, is plotted for the three different CO_2/CH_4 mixtures at a flow rate of 4 L/min. Additionally, Figure 4 D depicts the 1D calculated gas temperature profiles in the three gas mixtures, along a straight axial line in the center of the RGA reactor. These figures show that the gas temperature reaches up to almost 2500 K inside the plasma and cools down to around 800 K once the gas has left the reactor. Obviously, the gas temperature in the plasma decreases when more CH_4 is present in the mixture, from a peak gas temperature of almost 2500 to 2100 K, when the gas mixture is changed from 75/25 CO_2/CH_4 to 60/40 CO_2/CH_4, while the shape of the temperature profile itself remains unchanged. A higher gas

achieved a lower conversion with a higher energy cost of 5.9 eV/molecule. Significantly higher conversions of 52.3 and 58.9% for CO_2 and CH_4, respectively, were achieved by the "alternating current gliding arc" (AC-GA) reactor of Xia et al.,[15] but at a higher energy cost of 6.5 eV/molecule, which is almost twice as high as the energy cost in our reactor. The best results up to now in literature for a gliding arc reactor, to our knowledge, are reported for another RGA reactor by Wu et al.,[18] achieving a higher conversion of 36 and 35% for CO_2 and CH_4, respectively, at a very low energy cost of 1.5 eV/molecule. However, it should be noted that this reactor uses a magnetic field to enhance the plasma and improve the performance, which is a more complex setup and due to its additional costs, thus less viable for industrial applications. The fact that the performance of our reactor is on par or even better than similar RGA reactors truly demonstrates the strengths and benefits of the RGA design, capturing the arc within a rotating gas flow that drags the arc along in a rotating movement,

Table 1. Key Performance Indicators for DRM, Comparing Our Best Results with Different Types of Gliding Arc Plasmas from Literature

Reactor type	Gas mixture	CO_2 conversion (%)	CH_4 conversion (%)	EC (eV/molecule)	Ref
RGA	75/25 CO_2/CH_4	22.1	38.6	3.25	This work
GAP	75/25 CO_2/CH_4	18	10	2.5	17
RGA	50/0 CO_2/CH_4	12.8	10.9	14.4[a]	14
RGAD	60/40 CO_2/CH_4	17.0	28.1	5.9[a]	13
AC-GA	75/25 CO_2/CH_4	52.3	58.9	6.5[a]	15
RGA	50/50 CO_2/CH_4	36	35	1.53[a]	18
MW	70/30 CO_2/CH_4	49.4	66.5	2.8	11
APGD	75/25 CO_2/CH_4	64	94	4	9
DBD	50/50 CO_2/CH_4	44	73	140	50

[a]Value not provided in the reference but calculated using the provided data.
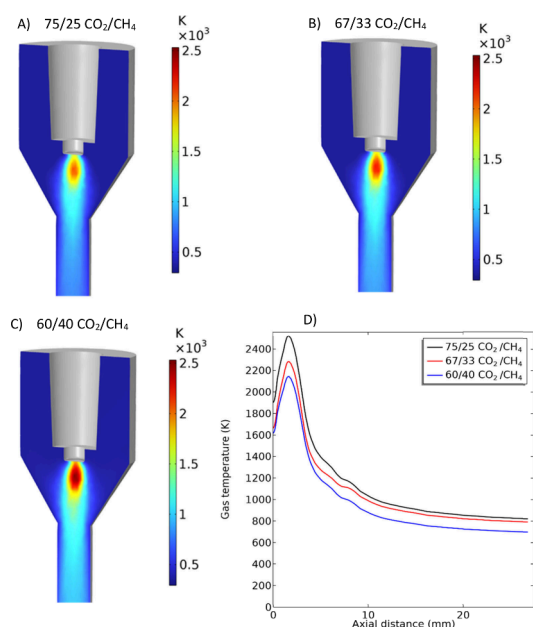
Figure 4. Gas temperature profiles in the RGA reactor, for (A) 75/25, (B) 67/33, and (C) 60/40 CO_2/CH_4 mixtures, as calculated by the 3D CFD model. (D) 1D axial temperature profiles along a straight line in the reactor for the three gas mixtures, to allow easy comparison.

Figure 5. Calculated Cp as a function of gas temperature for the three different CO_2/CH_4 mixtures. The calculated Cp for pure CO_2 is shown as a reference.

temperature results in faster chemical kinetics and thus the creation of more active species. The difference between 2100 and 2500 K in the center of the plasma results in a 3-fold increase in the forward reaction rate coefficient of the CO formation reaction ($CO_2 + H \rightarrow CO + OH$), due to the exponential dependence of this reaction rate coefficient on the temperature, explaining why the highest conversions are observed in the hotter 75/25 CO_2/CH_4 plasma.

The reason for the higher gas temperatures at lower CH_4 fractions is attributed to the fact that CH_4 molecules (and generally also their reaction products) have more internal degrees of freedom (vibrational and rotational) than CO_2 molecules. In a quasi-thermal plasma, like our RGA reactor, where relaxation between the various degrees of freedom within the molecules is very fast and all degrees of freedom are equally excited (i.e., $T_g = T_{trans} \approx T_{vib} \approx T_{rot}$), this means that more energy is lost to other degrees of freedom (i.e., vibration and rotation), rather than to the translational degree of freedom, yielding lower gas temperatures upon increasing CH_4 fraction in the mixture. This property is illustrated by the heat capacity of the mixture at constant pressure (Cp), as it represents the amount of energy that needs to be added to the gas to increase its gas temperature by 1K.

Figure 5 presents Cp of the three different CO_2/CH_4 ratios for a wide range of gas temperatures, as calculated by eq 17 in section 3.3. As a reference, the calculated Cp for pure CO_2 is also plotted. The figure clearly shows that for a higher amount of CH_4, the heat capacity increases, meaning that, indeed, more energy is required to increase the gas temperature when CH_4 is added. As very similar amounts of powers were used in the experiments for the different gas mixtures and similar energy costs and energy efficiencies were achieved (cf. Figure 7 in the following section), more CH_4 in the mixture thus yields a lower gas temperature and thus, as a result of slower chemical kinetics, lower conversion values.
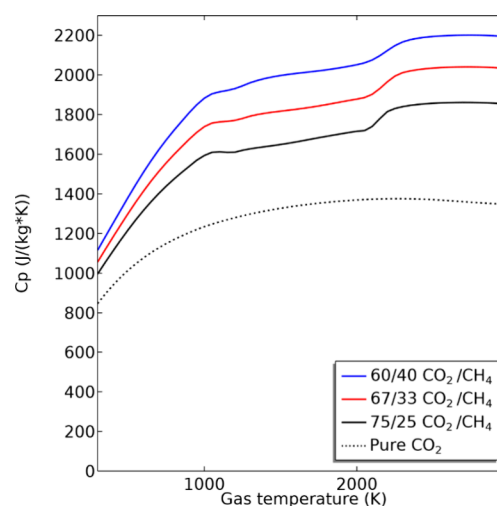
To verify our model predictions that a higher CO_2/CH_4 ratio leads to higher temperatures, we measured the temperature after the plasma with a thermocouple. This is not directly applicable to the plasma temperature, as the latter is much higher, but we could not obtain direct information about the plasma temperature. Indeed, the RGA reactor (stainless steel) does not allow optical emission spectroscopy, and an IR camera only provides information about the outside reactor walls, which is also not representative for the actual plasma temperature. Figure 6 presents the gas temperature at a distance of 3 cm from the reactor outlet, measured with a thermocouple, for all conditions. Even though the differences between the conditions are not very large, we can see that for all flow rates, the temperature is consistently lower at a higher CH_4 fraction. Although these measurements are only indicative, we see a consistent trend, so we believe these results can support our model predictions.

4.3. Maximizing the Energy Efficiency through CO Production. Figure 7 A and B present the measured energy efficiency and energy cost of the CO_2 and CH_4 conversion reaction in the RGA for the three different CO_2/CH_4 mixtures at the three different gas flow rates. Just like for the conversion, the figure shows that the highest energy efficiency of 62% is achieved at the lowest flow rate of 4 L/min for a 75/25 CO_2/CH_4 mixture. Note that this energy efficiency is much higher than the value of ±30% that is usually achieved for pure CO_2 conversion in atmospheric pressure GA reactors.[3,23] Indeed, this is attributed to the fact that the H atoms, that are created in the plasma from CH_4, are reactive enough to react with the stable CO_2 molecules, lowering the energy required to break the C = O bond. Furthermore, these values are higher than the energy efficiency target of 60% and energy cost of 4.27 eV/molecule that are defined by Snoeckx and Bogaerts for plasma-based CO_2 conversion and DRM to be competitive with other emerging CO_2 conversion technologies.[3]

It should also be noted that in Figure 5 A and B, a higher energy efficiency does not translate to a low energy cost. Indeed, while the highest energy efficiency of 62% is found at a flow rate of 4 L/min for a 75/25 CO_2/CH_4 mixture, the lowest energy cost of 2.6 eV/molecule is found at a higher flow rate, i.e. at 8 L/min for a 75/25 CO_2/CH_4 mixture. While the
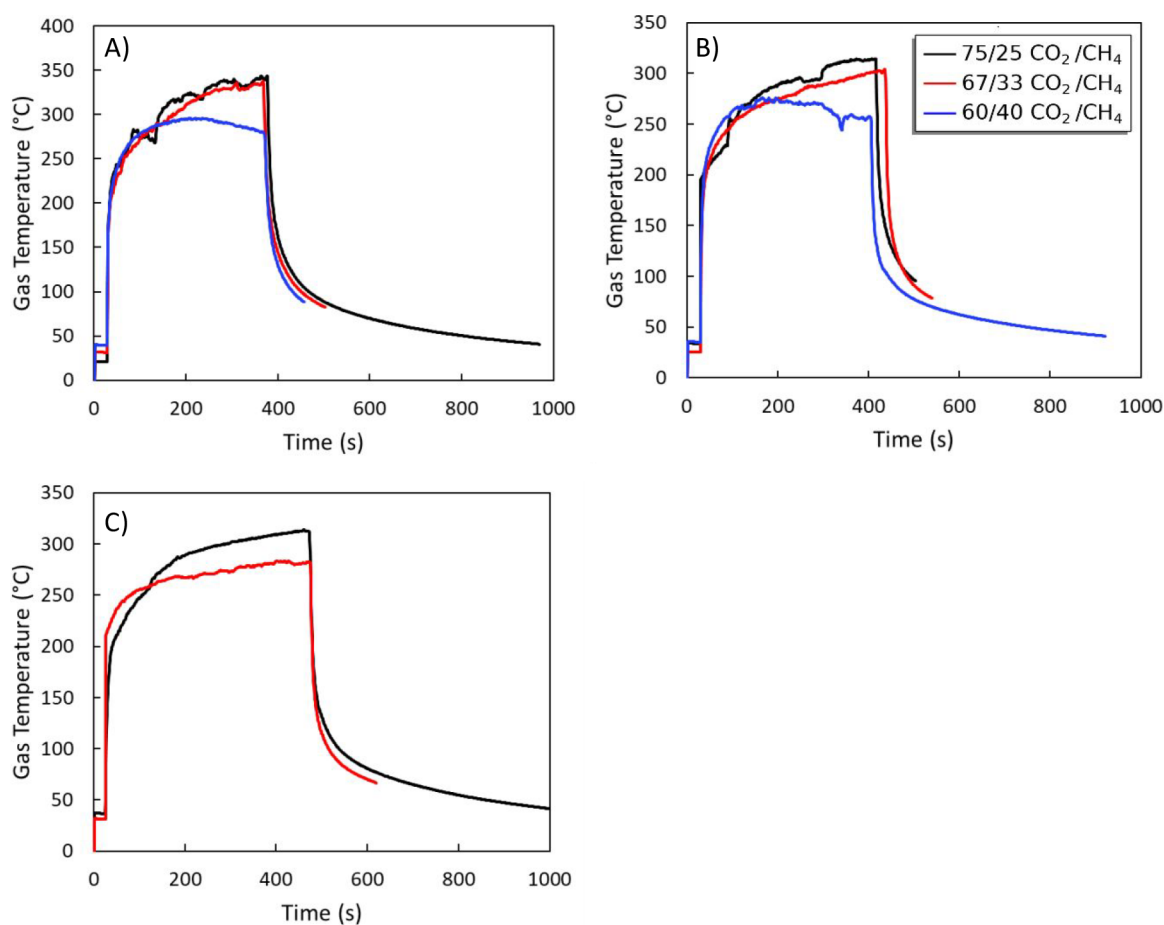
Figure 6. Temperature measured at ± 3 cm from the reactor outlet for each mixture, at (A) 4 L/min, (B) 6 L/min and (C) 8 L/min.

energy cost purely defines the amount of energy that goes into the process, being inversely proportional to the flow rate (see eqs 8 and 9), the energy efficiency, as defined in eq 10, shows how efficiently the consumed energy is used to break and create chemical bonds and convert CO_2 and CH_4 into value-added products. As shown by eq 10, this definition of the energy efficiency is highly dependent on the concentration of the major end products, i.e. CO and H_2. The concentration of these products is plotted in Figure 8, in the three different CO_2/CH_4 mixtures for the three different gas flow rates. It should be mentioned that some other components, i.e. C_2H_2 and C_2H_4, are also qualitatively measured. The direct formation of these higher-value hydrocarbons is very beneficial for future industrial applications. However, Figure 9 displays the carbon balance based on the CO_2, CH_4 and CO concentrations for all conditions, confirming that no other carbon-based products are formed in significant amounts.

Figure 8 shows that higher CO and H_2 concentrations are achieved at lower flow rates, due to the higher residence time in the plasma when the gas flows more slowly through the reactor. As a result, a higher overall energy efficiency is achieved at lower flow rates, even though the energy cost is higher. In Figure 7 A, the fact that the highest energy efficiency is achieved at lower CH_4 concentration is attributed to the higher CO_2 and CH_4 conversions obtained for this mixture (see Figure 3), using the same power input. Additionally, purely from an energy efficiency standpoint, this gas mixture also has the most beneficial product distribution. From Figure

8 it is obvious that a higher CO_2 content in the feed gas favors CO formation, while higher CH_4 contents favor the formation of H_2. Therefore, purely from an energy efficiency standpoint, maximizing the CO concentration is most beneficial, as splitting CO_2 into CO is the most energy-intensive process from a chemical point of view, as opposed to forming H_2 out of CH_4. The latter follows directly from the enthalpy (or LHV, defined in eq 10) differences between reactant and product of these two reactions, which is, as illustrated by eq 10 of section 2.2, an important factor in the calculation of the energy efficiency. This means that it is more favorable for the energy efficiency that H-based radicals, which are formed from CH_4 in the plasma, break the strong CO_2 bond and help the very endothermic CO formation, rather than react with each other to form e.g. H_2. This occurs mostly when the concentrations of these H atoms in the plasma are not too high, i.e. at lower CH_4 concentrations.

The latter is also verified by our model. Indeed, Figure 10 illustrates the calculated equilibrium molar fraction of CO for the three different CO_2/CH_4 gas mixtures in a wide range of gas temperatures, as well as the molar fraction of CO in case of pure CO_2 splitting, as a reference. The figure shows that adding CH_4 to pure CO_2 greatly improves the CO formation (cf. the pure CO_2 curve and the 75/25 CO_2/CH_4 curve), as it enables CO production from temperatures as low as 1000 K, by providing H-based radicals (like H, CH, OH and HCO) that enable new and efficient CO formation pathways. However, while the presence of these radicals initially improves
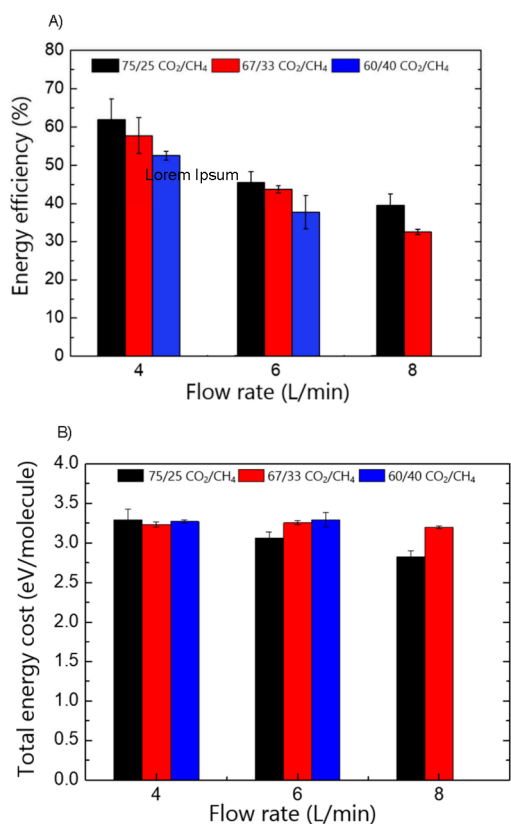
Figure 7. Measured energy efficiency (A) and energy cost (B), for the three different CO_2/CH_4 mixtures at gas flow rates of 4,6 and 8 L/min.

Figure 9. Carbon balance accounting for CO_2, CH_4, and CO for the three different CO_2/CH_4 mixtures, at gas flow rates of 4, 6, and 8 L/min.
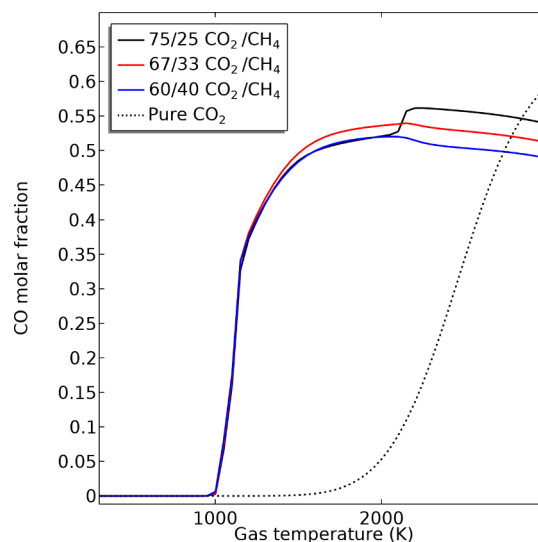
Figure 10. Calculated CO molar fraction as a function of gas temperature for the three different CO_2/CH_4 mixtures, as well as for pure CO_2 splitting, as a reference.

the CO formation, Figure 10 also shows that further increasing the CH_4 content, and thus increasing the concentration of these radicals, does not further improve the CO formation, but rather leads to a decrease in CO formation. As explained above, this is attributed to the fact that at high concentrations, these H atoms react with each other, forming H_2, rather than reacting with CO_2. Furthermore, at higher CO_2 concentrations, a significant amount of CO is still formed through the thermal CO_2 splitting pathway, $CO_2 + M \rightarrow CO + O$, with M any neutral collision partner. Most of the time this is an O radical, as this the most reactive reaction partner. This reaction only becomes significant at elevated temperature, i.e. around 2000 K. This is visible in Figure 10 as a slight increase in CO fraction at 2000 K for the 75/25 CO_2/CH_4 ratio. This is also the temperature where the CO formation becomes significant

for the pure CO_2 condition in Figure 10, as this is the only available CO-formation pathway at this condition. This pathway becomes less significant as the CH_4 fraction increases, as the O radicals, which are the most reactive collision partner (M) for the pure CO_2 splitting process, quickly recombine with H-based radicals from CH_4 dissociation, which is further elaborated in next section.

Hence, to maximize the energy efficiency, our model predicts that CH_4 should be present to improve the CO

Figure 8. Measured (A) CO and (B) H_2 concentrations, for the three different CO_2/CH_4 mixtures, at gas flow rates of 4,6 and 8 L/min.
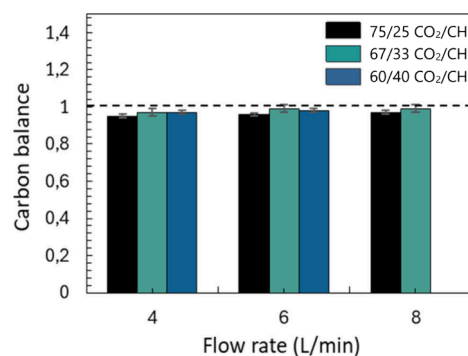
formation process, but its concentration should not be too high, in line with our Experimental Data.

4.4. H-Based Radicals As Recombination Suppressors.

As discussed in section 4.2, the addition of CH_4 introduces chemical pathways to produce H_2, C_2H_2 and C_2H_4, but also delivers more pathways to split CO_2 into CO, through reactions between CO_2 and H-based radicals. Additionally, these H-based radicals not only influence the CO formation inside the plasma, but also the CO recombination after the plasma. Indeed, a significant problem for CO_2 conversion in quasi-thermal plasmas is that the process suffers from CO recombination reactions when the gas cools down after the plasma.[51,52] Indeed, the O atoms (or O_2 molecules), produced by CO_2 splitting, react with the formed CO after the plasma, reversing the CO_2 splitting process and recombining into CO_2. Our computational models suggest that these back-reactions are reduced when CH_4 is added to the mixture, as the H radicals, originating from CH_4 dissociation, react with the O atoms, removing the latter before they can recombine with CO. These reactions are schematically illustrated in Figure 11. The figure clearly illustrates the two

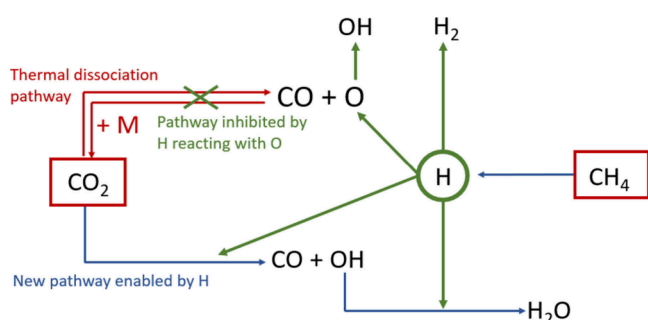**Figure 11.** Reduced schematic representation of the reaction pathways of the CO_2/CH_4 plasma chemistry, illustrating the role of H radicals, originating from CH_4 dissociation, in (i) inhibiting the thermal CO_2 dissociation pathway, as well as its reverse reaction, i.e., recombination of CO with O, as it quickly recombines with the O radicals, and (ii) creating a new CO_2 dissociation pathway upon collision of CO_2 with H radicals

dissociation pathways of CO_2: (i) the thermal dissociation pathway, in which CO_2 dissociates upon collision with another species M (which most of the time is an O radical, as this the most reactive reaction partner) and (ii) the dissociation pathway enabled by H radicals, originating from CH_4 dissociation. As discussed in previous section, this second pathway allows for CO_2 dissociation at a lower gas temperature. As the recombination of CO to CO_2 (reverse red arrow) requires the presence of O radicals, this pathway is inhibited by the H radicals, originating from CH_4 dissociation, which recombine quickly with O to form OH. Note that this also inhibits the forward thermal dissociation pathway, as the reaction relies on O, as the main collision partner M.

The inhibition of the CO recombination reaction is further illustrated in Figure 12 a), by plotting the calculated CO_2 and CH_4 conversion along a straight line in the center of the reactor, for the 75/25 and 60/40 CO_2/CH_4 mixtures. The intermediate (67/33) mixture is not depicted, for the sake of clarity. These time-based evolutions are calculated with our quasi-1D chemical kinetics model, which simulates the CO_2 and CH_4 chemistry as the gas flows along a straight line in the center of the reactor, using the gas flow velocities and gas temperatures calculated by the 3D gas flow model as input, as explained in section 3.4. For both gas mixtures, Figure 12 a) clearly shows the influence of the plasma at about 0.3 ms, indicated by a steep rise in both CH_4 and CO_2 conversion. As explained in section 4.1, the CO_2 and CH_4 conversion reach higher values in the 75/25 CO_2/CH_4 gas mixture, due to the higher gas temperature. However, in this mixture the CO_2 conversion decreases slightly after reaching a peak inside the plasma, as the gas cools down and CO recombination reactions kick in. In the 60/40 CO_2/CH_4 gas mixture, however, this drop in CO_2 conversion is not present, as the O atoms instantly react with H-based radicals, which are more abundant in this mixing ratio, and they are also more reactive than CO, "freezing" the CO_2 conversion as it was achieved in the plasma. This is illustrated in Figure 12 b), displaying the rate of the recombination reaction between O and H, removing the O radicals ($O + H + M \rightarrow OH + M$, in which M represents any neutral collision partner) along the same time evolution. This figure shows that for the 60/40 CO_2/CH_4 ratio, the O radical scavenging reaction occurs at a much higher rate, thus
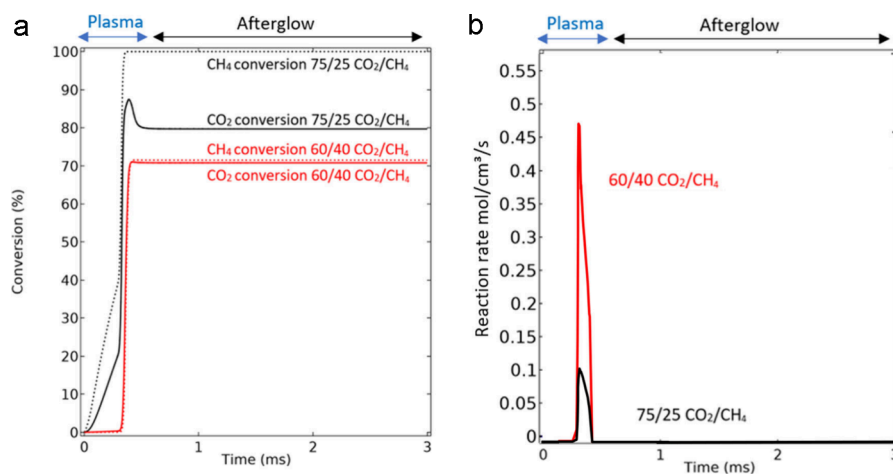

Figure 12. a) Time evolution of the CO_2 and CH_4 conversion throughout the plasma and afterglow, and b) Reaction rate of the oxygen scavenging reaction ($O + H + M \rightarrow OH + M$), in a 75/25 and 60/40 CO_2/CH_4 mixture, as calculated by our quasi-1D chemical kinetics model, showing that the rate of this reaction is much higher at higher CH_4 fractions in the mixture.

removing O radicals that can cause the recombination reaction with CO. Therefore, even though the increased CO retention in the 60/40 CO_2/CH_4 mixture cannot compensate for the lower conversion attributed to the lower gas temperature in this mixture, as discussed in section 4.1, it does enable CH_4 as an interesting molecule for suppressing CO recombination in future work, using H-based radicals as an in situ scavenging molecule, as was also reported in earlier work.[53]

5. CONCLUSION

In this work we present the performance of an RGA plasma reactor for CO_2 and CH_4 conversion, yielding a maximum CO_2 conversion of 22% and a CH_4 conversion of 39%, at an energy efficiency of 62% and energy cost of 3.25 eV/molecule, for a 75/25 CO_2/CH_4 gas mixture at a flow rate of 4 L/min. At 8 L/min, the energy cost and energy efficiency were slightly lower (2.6 eV/molecule and 40%, respectively). These results are quite competitive compared to other (gliding arc) plasma reactors.

To better understand the observed trends, we developed both a 3D CFD model and quasi-1D chemical kinetics model. Our computational models predict that the addition of CH_4 increases the overall heat capacity of the gas mixture, thus yielding a somewhat lower gas temperature inside the plasma. As higher gas temperatures result in faster chemical kinetics, this explains our experimental data, in which the gas mixture with the least amount of CH_4 (i.e., 75/25 CO_2/CH_4) yields the highest CO_2 and CH_4 conversion. Additionally, the 75/25 CO_2/CH_4 mixture also exhibits the highest energy efficiency and lowest energy cost, due to the high conversion, as well as due to the high CO concentrations in this gas mixture, which is the most beneficial product in terms of energy efficiency.

On the other hand, while a lower CH_4 fraction yields the most favorable results, the addition of small amounts of CH_4 is quite important to achieve high conversion values, as H-based radicals formed from CH_4 introduce more efficient CO formation pathways compared to pure CO_2 splitting. It is only when the concentration of these H-based radicals becomes too high, that the recombination of these radicals with each other becomes more important than their reaction with CO_2, yielding lower conversion. Additionally, our computational models also show that the addition of CH_4 suppresses CO recombination reactions after the plasma, as H-based radicals quickly react with O atoms, that would otherwise recombine with CO to form CO_2 again. While this effect has a positive influence on the CO retention at higher CH_4 concentration, it cannot compensate for the lower conversion attributed to the lower gas temperature in these conditions.

The insights obtained by our models are not only useful to explain our experimental data, but can also be used in future work to further tune the process toward optimal conversion and energy efficiency. To expand the conclusions of our study, additional model calculations will be needed, covering a broader range of compositions, and subsequently validating these findings experimentally. This will further enhance the robustness and applicability of our research outcomes.

ASSOCIATED CONTENT

Ⓢ Supporting Information

The Supporting Information is available free of charge at https://pubs.acs.org/doi/10.1021/acssuschemeng.4c06627.

I−V profiles of all experimental conditions used in this research (PDF)

■ AUTHOR INFORMATION

Corresponding Authors

Senne Van Alphen − *Department of Chemistry, Research Group PLASMANT, University of Antwerp, 2610 Wilrijk, Belgium;* ⊙ orcid.org/0000-0003-0870-1453; Email: senne.vanalphen@uantwerpen.be

Annemie Bogaerts − *Department of Chemistry, Research Group PLASMANT, University of Antwerp, 2610 Wilrijk, Belgium;* ⊙ orcid.org/0000-0001-9875-6460; Email: annemie.bogaerts@uantwerpen.be

Authors

Bart Wanten − *Department of Chemistry, Research Group PLASMANT, University of Antwerp, 2610 Wilrijk, Belgium;* ⊙ orcid.org/0000-0002-0802-1530

Fanny Girard-Sahun − *Department of Chemistry, Research Group PLASMANT, University of Antwerp, 2610 Wilrijk, Belgium*

Joachim Slaets − *Department of Chemistry, Research Group PLASMANT, University of Antwerp, 2610 Wilrijk, Belgium;* ⊙ orcid.org/0000-0001-9536-0444

James Creel − *Department of Chemistry, Research Group PLASMANT, University of Antwerp, 2610 Wilrijk, Belgium*

Maryam Aghaei − *Department of Chemistry, Research Group PLASMANT, University of Antwerp, 2610 Wilrijk, Belgium;* ⊙ orcid.org/0000-0003-4995-8773

Complete contact information is available at: https://pubs.acs.org/10.1021/acssuschemeng.4c06627

Author Contributions

§S.V.A., B.W., F.G.-S., and J.S. contributed equally to the paper.

Notes

The authors declare no competing financial interest.

■ REFERENCES

(1) Pachauri, R. K.; Meyer, L. A. Climate Change 2014: Synthesis Report. Contribution of Working Groups I, II and III to the Fifth Assessment Report of the Intergovernmental Panel on Climate Change, Geneva, Switzerland, 2014; 2014.

(2) Arora, S.; Prasad, R. An Overview on Dry Reforming of Methane: Strategies to Reduce Carbonaceous Deactivation of Catalysts. *RCS Advances* **2016**, *6* (110), 108668−108688.

(3) Snoeckx, R.; Bogaerts, A. Plasma Technology-a Novel Solution for CO2 Conversion? *Chem. Soc. Rev.* **2017**, *46* (19), 5805−5863.

(4) Singh, R.; Dhir, A.; Kumar Mohapatra, S.; Kumar Mahla, S. Dry Reforming of Methane Using Various Catalysts in the Process: Review. *Biomass Convers Biorefin* **2020**, *10*, 567−587.

(5) Fridman, A. *Plasma Chemistry*; Cambridge University Press: Cambridge, U.K., 2008. DOI: 10.1017/CBO9780511546075.

(6) Scapinello, M.; Martini, L. M.; Tosi, T. CO2 Hydrogenation by CH4 in a Dielectric Barrier Discharge: Catalytic Effect of Ni and Cu. *Plasma Processes Polym.* **2014**, *11*, 624−628.

(7) Wang, L.; Yi, Y.; Wu, C.; Guo, H.; Tu, X. One-Step Reforming of CO2 and CH4 into High-Value Liquid Chemicals and Fuels at Room Temperature by Plasma-Driven Catalysis. *Angewandte Chemie - International Edition* **2017**, *56* (44), 13679−13683.

(8) Li, D.; Li, X.; Bai, M.; Tao, X.; Shang, S.; Dai, X.; Yin, Y. CO2 Reforming of CH4 by Atmospheric Pressure Glow Discharge Plasma: A High Conversion Ability. *Int. J. Hydrogen Energy* **2009**, *34*, 308−313.

(9) Wanten, B.; Maerivoet, S.; Vantomme, C.; Slaets, J.; Trenchev, G.; Bogaerts, A. Dry Reforming of Methane in an Atmospheric Pressure Glow Discharge: Confining the Plasma to Expand the Performance. *Journal of CO2 Utilization* **2022**, *56*, 56.

(10) Jasiński, M.; Dors, M.; Mizeraczyk, J. Production of Hydrogen via Methane Reforming Using Atmospheric Pressure Microwave Plasma. *J. Power Sources* **2008**, *181* (1), 41−45.

(11) Kelly, S.; Mercer, E.; De Meyer, R.; Ciocarlan, R. G.; Bals, S.; Bogaerts, A. Microwave Plasma-Based Dry Reforming of Methane: Reaction Performance and Carbon Formation. *Journal of CO2 Utilization* **2023**, *75*, 75.

(12) Biondo, O.; van Deursen, C. F. A. M.; Hughes, A.; van de Steeg, A.; Bongers, W.; van de Sanden, M. C. M.; van Rooij, G.; Bogaerts, A. Avoiding Solid Carbon Deposition in Plasma-Based Dry Reforming of Methane. *Green Chem.* **2023**, *25* (24), 10485−10497.

(13) Lu, N.; Sun, D.; Xia, Y.; Shang, K.; Wang, B.; Jiang, N.; Li, J.; Wu, Y. Dry Reforming of CH4-CO2 in AC Rotating Gliding Arc Discharge: Effect of Electrode Structure and Gas Parameters. *Int. J. Hydrogen Energy* **2018**, *43* (29), 13098−13109.

(14) Martin-del-Campo, J.; Coulombe, S.; Kopyscinski, J. Influence of Operating Parameters on Plasma-Assisted Dry Reforming of Methane in a Rotating Gliding Arc Reactor. *Plasma Chemistry and Plasma Processing* **2020**, *40* (4), 857−881.

(15) Xia, Y.; Lu, N.; Wang, B.; Li, J.; Shang, K.; Jiang, N.; Wu, Y. Dry Reforming of CO2-CH4 Assisted by High-Frequency AC Gliding Arc Discharge: Electrical Characteristics and the Effects of Different Parameters. *Int. J. Hydrogen Energy* **2017**, *42* (36), 22776−22785.

(16) Slaets, J.; Aghaei, M.; Ceulemans, S.; Van Alphen, S.; Bogaerts, A. CO2 and CH4 Conversion in "Real" Gas Mixtures in a Gliding Arc Plasmatron: How Do N2 and O2 Affect the Performance? *Green Chem.* **2020**, *22* (4), 1366−1377.

(17) Cleiren, E.; Heijkers, S.; Ramakers, M.; Bogaerts, A. Dry Reforming of Methane in a Gliding Arc Plasmatron: Towards a Better Understanding of the Plasma Chemistry. *ChemSusChem* **2017**, *10* (20), 3864−3864.

(18) Wu, A.; Yan, J.; Zhang, H.; Zhang, M.; Du, C.; Li, X. Study of the Dry Methane Reforming Process Using a Rotating Gliding Arc Reactor. *Int. J. Hydrogen Energy* **2014**, *39* (31), 17656−17670.

(19) Tu, X.; Whitehead, J. C. Plasma Dry Reforming of Methane in an Atmospheric Pressure AC Gliding Arc Discharge: Co-Generation of Syngas and Carbon Nanomaterials. *Int. J. Hydrogen Energy* **2014**, *39* (18), 9658−9669.

(20) Fridman, A.; Chirokov, A.; Gutsol, A. Non-Thermal Atmospheric Pressure Discharges. *J. Phys. D Appl. Phys.* **2005**, *38* (2), R1−R24.

(21) Fridman, A.; Gutsol, A.; Gangoli, S.; Ju, Y.; Ombrello, T. Characteristics of Gliding Arc and Its Application in Combustion Enhancement. *J. Propuls Power* **2008**, *24* (6), 1216−1228.

(22) Nunnally, T; Gutsol, K; Rabinovich, A; Fridman, A; Gutsol, A; Kemoun, A Dissociation of CO2 in a Low Current Gliding Arc Plasmatron. *J. Phys. D Appl. Phys.* **2011**, *44*, 274009.

(23) Ramakers, M.; Trenchev, G.; Heijkers, S.; Wang, W.; Bogaerts, A. Gliding Arc Plasmatron: Providing an Alternative Method for Carbon Dioxide Conversion. *ChemSusChem* **2017**, *10* (12), 2642−2652.

(24) Gröger, S.; Ramakers, M.; Hamme, M.; Medrano, J. A.; Bibinov, N.; Gallucci, F.; Bogaerts, A.; Awakowicz, P. Characterization of a Nitrogen Gliding Arc Plasmatron Using Optical Emission Spectroscopy and High-Speed Camera. *J. Phys. D Appl. Phys.* **2019**, *52* (6), 065201.

(25) Trenchev, G.; Kolev, S.; Wang, W.; Ramakers, M.; Bogaerts, A. CO2 Conversion in a Gliding Arc Plasmatron: Multidimensional Modeling for Improved Efficiency. *J. Phys. Chem. C* **2017**, *121* (39), 24470−24479.

(26) Zhang, H.; Zhu, F.; Li, X.; Du, C. Dynamic Behavior of a Rotating Gliding Arc Plasma in Nitrogen: Effects of Gas Flow Rate and Operating Current. *Plasma Science and Technology* **2017**, *19* (4), 045401.

(27) Zhang, H.; Wang, W.; Li, X.; Han, L.; Yan, M.; Zhong, Y.; Tu, X. Plasma Activation of Methane for Hydrogen Production in a N2 Rotating Gliding Arc Warm Plasma: A Chemical Kinetics Study. *Chemical Engineering Journal* **2018**, *345* (March), 67−78.

(28) Zhao, T.-L.; Liu, J.-L.; Li, X.-S.; Liu, J.-B.; Song, Y.-H.; Xu, Y.; Zhu, A.-M. Dynamic Evolution of 50-Hz Rotating Gliding Arc Discharge in a Vortex Air Flow. *IEEE Transactions on Plasma Science* **2014**, *42* (10), 2704−2705.

(29) Kuznetsova, I. V.; Kalashnikov, N. Y.; Gutsol, A. F.; Fridman, A. A.; Kennedy, L. A. Effect of "Overshooting" in the Transitional Regimes of the Low-Current Gliding Arc Discharge. *J. Appl. Phys.* **2002**, *92* (8), 4231−4237.

(30) Zhang, H.; Li, X. D.; Zhang, Y. Q.; Chen, T.; Yan, J. H.; Du, C. M. Rotating Gliding Arc Codriven by Magnetic Field and Tangential Flow. *IEEE Transactions on Plasma Science* **2012**, *40* (12), 3493−3498.

(31) Lee, D. H.; Kim, K.-T.; Cha, M. S.; Song, Y.-H. Optimization Scheme of a Rotating Gliding Arc Reactor for Partial Oxidation of Methane. *Proceedings of the Combustion Institute* **2007**, *31* (2), 3343−3351.

(32) Van Alphen, S.; Jardali, F.; Creel, J.; Trenchev, G.; Snyders, R.; Bogaerts, A. Sustainable Gas Conversion by Gliding Arc Plasmas: A New Modelling Approach for Reactor Design Improvement. *Sustain Energy Fuels* **2021**, *5*, 1786−1800.

(33) Van Alphen, S.; Ahmadi Eshtehardi, H.; O'Modhrain, C.; Bogaerts, J.; Van Poyer, H.; Creel, J.; Delplancke, M.-P.; Snyders, R.; Bogaerts, A. Effusion Nozzle for Energy-Efficient NOx Production in a Rotating Gliding Arc Plasma Reactor. *Chemical Engineering Journal* **2022**, *443*, 136529.

(34) Jardali, F.; Van Alphen, S.; Creel, J.; Ahmadi Eshtehardi, H.; Axelsson, M.; Ingels, R.; Snyders, R.; Bogaerts, A. NOxproduction in a Rotating Gliding Arc Plasma: Potential Avenue for Sustainable Nitrogen Fixation. *Green Chem.* **2021**, *23* (4), 1748−1757.

(35) Wanten, B.; Vertongen, R.; De Meyer, R.; Bogaerts, A. Plasma-Based CO2 Conversion: How to Correctly Analyze the Performance? *Journal of Energy Chemistry* **2023**, *86*, 180−196.

(36) Pinhão, N.; Moura, A.; Branco, J. B.; Neves, J. Influence of Gas Expansion on Process Parameters in Non-Thermal Plasma Plug-Flow Reactors: A Study Applied to Dry Reforming of Methane. *Int. J. Hydrogen Energy* **2016**, *41* (22), 9245−9255.

(37) *COMSOL Multiphysics® v. 6.0*, COMSOL AB: Stockholm, Sweden.

(38) Van Alphen, S.; Hecimovic, A.; Kiefer, C. K.; Fantz, U.; Snyders, R.; Bogaerts, A. Modelling Post-Plasma Quenching Nozzles for Improving the Performance of CO2Microwave Plasmas. *Chemical Engineering Journal* **2023**, *462*, 462.

(39) Wolf, A. J.; Righart, T. W.; Peeters, F. J.; Bongers, W. A.; van de Sanden, M. C. Implications of Thermo-Chemical Instability on the Contracted Modes in CO2Microwave Plasmas. *Plasma Sources Sci. Technol.* **2020**, *29*, 025005.

(40) Van Den Bekerom, D. C. M.; Linares, J. M. P.; Verreycken, T.; Van Veldhuizen, E. M.; Nijdam, S.; Berden, G.; Bongers, W. A.; Van De Sanden, M. C. M.; Van Rooij, G. J. The Importance of Thermal Dissociation in CO2Microwave Discharges Investigated by Power Pulsing and Rotational Raman Scattering. *Plasma Sources Sci. Technol.* **2019**, *28* (5), 055015.

(41) Smith, G. P.; Golden, D. M.; Frenklach, M.; Moriarty, N. W.; Eiteneer, B.; Goldenberg, M.; Bowman, T. C.; Hanson, R. K.; Song, S.; Gardiner, W. C.; Lissianski, V. V.; Qin, Z. *GRI-MECH 3.0*. http://www.me.berkeley.edu/gri_mech/.

(42) *Chemical Reaction Engineering Module, COMSOL Multiphysics*. COMSOL AB: Stockholm, Sweden, pp 34−56.

(43) Stiel, L. I.; Thodos, G. The Viscosity of Polar Substances in the Dense Gaseous and Liquid Regions. *AIChE J.* **1964**, *10* (2), 275−277.

(44) Brokaw, R. S. Predicting Transport Properties of Dilute Gases. *Industrial and Engineering Chemistry Process Design and Development* **1969**, *8* (2), 240−253.

(45) Neufeld, P. D.; Janzen, A. R.; Aziz, R. A. Empirical Equations to Calculate 16 of the Transport Collision Integrals $\Omega(l,8)^*$ for the Lennard-Jones (12−6) Potential. *J. Chem. Phys.* **1972**, *57* (3), 1100−1102.

(46) Wilke, C. R. A Viscosity Equation for Gas Mixtures. *J. Chem. Phys.* **1950**, *18* (4), 517−519.

(47) McBride, B. J.; Zehe, M. J.; Gordon, S. *NASA Glenn Coefficients for Calculating Thermodynamic Properties of Individual Species*: National Aeronautics and Space Administration; 2002.

(48) Bogaerts, A.; Centi, G. Plasma Technology for CO2 Conversion: A Personal Perspective on Prospects and Gaps. *Frontiers in Energy Research* **2020**, *8*, 111 DOI: 10.3389/fenrg.2020.00111.

(49) Bogaerts, A.; Neyts, E. C. Plasma Technology: An Emerging Technology for Energy Storage. *ACS Energy Lett.* **2018**, *3* (4), 1013−1027.

(50) Wang, Q.; Yan, B.-H.; Jin, Y.; Cheng, Y. Investigation of Dry Reforming of Methane in a Dielectric Barrier Discharge Reactor. *Plasma Chemistry and Plasma Processing* **2009**, *29* (3), 217−228.

(51) Vermeiren, V.; Bogaerts, A. Plasma-Based CO2 Conversion: To Quench or Not to Quench? *J. Phys. Chem. C* **2020**, *124* (34), 18401−18415.

(52) Hecimovic, A.; D'Isa, F. A.; Carbone, E.; Fantz, U. Enhancement of CO2 Conversion in Microwave Plasmas Using a Nozzle in the Effluent. *Journal of CO2 Utilization* **2022**, *57*, 101870.

(53) Aerts, R.; Snoeckx, R.; Bogaerts, A. In-Situ Chemical Trapping of Oxygen in the Splitting of Carbon Dioxide by Plasma. *Plasma Processes and Polymers* **2014**, *11* (10), 985−992.

Supporting information

The role of CH$_4$ in plasma-assisted CO$_2$ and CH$_4$ conversion in a rotating gliding arc plasma: Insights revealed by experiments and modeling

Senne Van Alphen[*§], Bart Wanten[§], Fanny Girard-Sahun[§], Joachim Slaets[§], James Creel,

Maryam Aghaei and Annemie Bogaerts[*]

Department of Chemistry, Research Group PLASMANT, University of Antwerp, Universiteitsplein 1, 2610 Wilrijk, Belgium
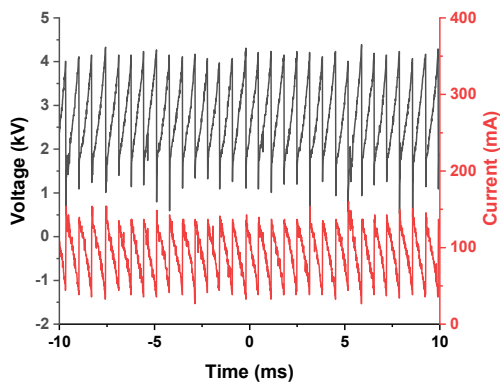
*corresponding authors

[§]These authors contributed equally to the paper

This supporting information contains the following figures:

- Figure S.1 presents the I-V profiles of all experimental conditions used in this research, further illustrating the explanation in section 4.1 of the main paper.

S.1 I-V profiles of all experimental conditions
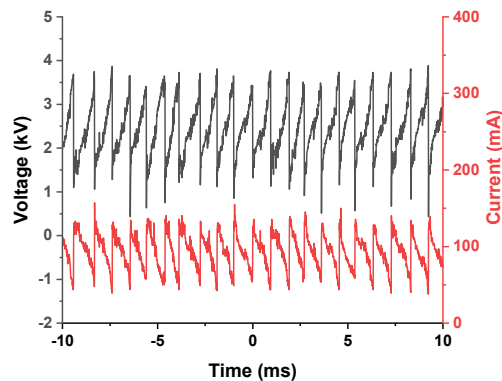
75/25 CO₂/CH₄ 4L/min
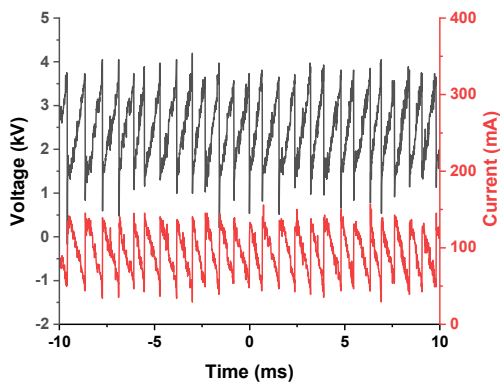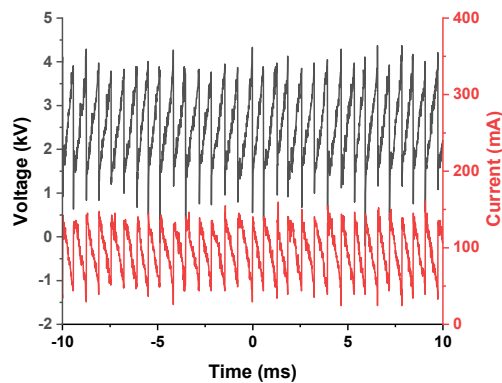
75/25 CO₂/CH₄ 6L/min
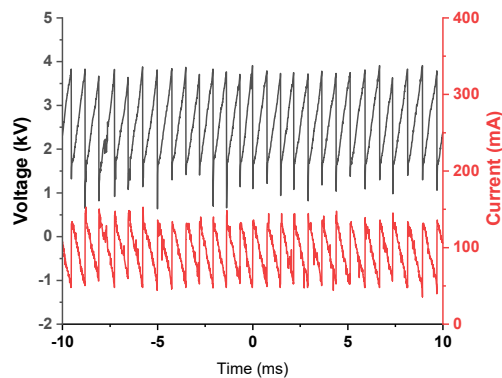
75/25 CO₂/CH₄ 8L/min
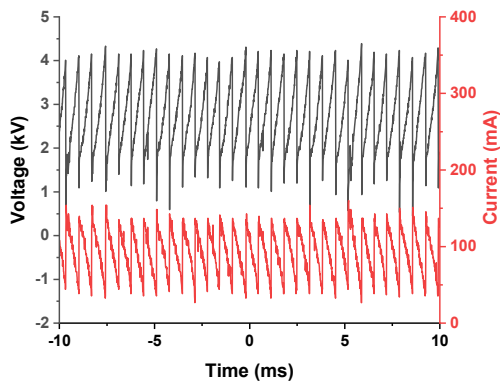
67/33 CO₂/CH₄ 4L/min

67/33 CO₂/CH₄ 6L/min

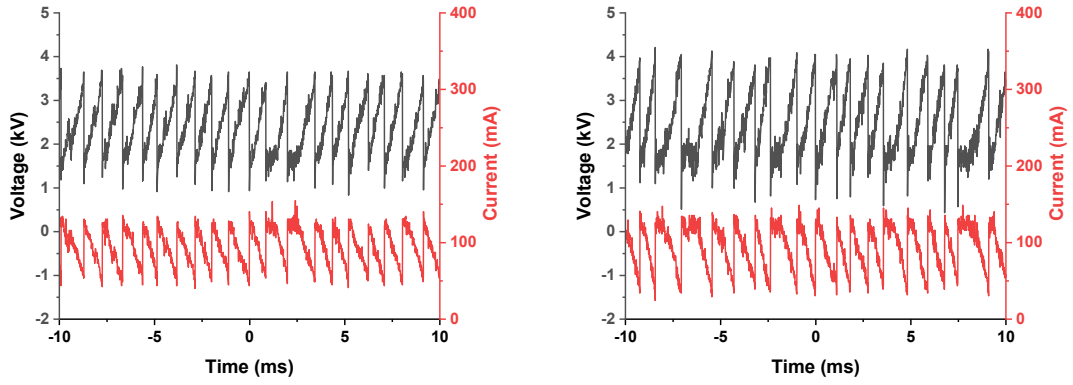67/33 CO₂/CH₄ 8L/min

60/40 CO₂/CH₄ 4L/min

60/40 CO₂/CH₄ 6L/min

Figure S.1: I-V profiles of all experimental conditions of the main paper.